Pergamon

Geochimica et Cosmochimica Acta, Vol. 65, No. 7, pp. 1269–1284, 2002

0016-7037/02 $22.00 + .00

PII S0016-7037(00)00772-4

Rare earth element variations resulting from inversion of pigeonite and subsolidus reequilibration in lunar ferroan anorthosites

ODETTE B. JAMES,[1]* CHRISTINE FLOSS,[2] and JAMES J. MCGEE[3],†

[1]Emeritus, 926A National Center, U.S. Geological Survey, Reston, VA 20192, USA
[2]Laboratory for Space Sciences and Department of Earth and Planetary Sciences, Washington University, St. Louis, MO 63130, USA
[3]Department of Geological Sciences, University of South Carolina, Columbia, SC 29208, USA

(*Received June* 20, 2000; *accepted in revised form July* 10, 2001)

Abstract—We present results of a secondary ion mass spectrometry study of the rare earth elements (REEs) in the minerals of two samples of lunar ferroan anorthosite, and the results are applicable to studies of REEs in all igneous rocks, no matter what their planet of origin. Our pyroxene analyses are used to determine solid–solid REE distribution coefficients ($D = C_{REE}$ in low-Ca pyroxene/C_{REE} in augite) in orthopyroxene–augite pairs derived by inversion of pigeonite. Our data and predictions from crystal-chemical considerations indicate that as primary pigeonite inverts to orthopyroxene plus augite and subsolidus reequilibration proceeds, the solid–solid Ds for orthopyroxene–augite pairs progressively decrease for all REEs; the decrease is greatest for the LREEs. The REE pattern of solid–solid Ds for inversion-derived pyroxene pairs is close to a straight line for Sm-Lu and turns upward for REEs lighter than Sm; the shape of this pattern is predicted by the shapes of the REE patterns for the individual minerals.

Equilibrium liquids calculated for one sample from the compositions of primary phases, using measured or experimentally determined solid–liquid Ds, have chondrite-normalized REE patterns that are very slightly enriched in LREEs. The plagioclase equilibrium liquid is overall less rich in REEs than pyroxene equilibrium liquids, and the discrepancy probably arises because the calculated plagioclase equilibrium liquid represents a liquid earlier in the fractionation sequence than the pyroxene equilibrium liquids. "Equilibrium" liquids calculated from the compositions of inversion-derived pyroxenes or orthopyroxene derived by reaction of olivine are LREE depleted (in some cases substantially) in comparison with equilibrium liquids calculated from the compositions of primary phases. These discrepancies arise because the inversion-derived and reaction-derived pyroxenes did not crystallize directly from liquid, and the use of solid–liquid Ds is inappropriate. The LREE depletion of the calculated liquids is a relic of formation of these phases from primary LREE-depleted minerals. Thus, if one attempts to calculate the compositions of equilibrium liquids from pyroxene compositions, it is important to establish that the pyroxenes are primary. In addition, our data suggest that experimental studies have underestimated solid–liquid Ds for REEs in pigeonite and that REE contents of liquids calculated using these Ds are overestimates.

Our results have implications for Sm-Nd age studies. Our work shows that if pigeonite inversion and/or subsolidus reequilibration between augite and orthopyroxene occurred significantly after crystallization, and if pyroxene separates isolated for Sm-Nd studies do not have the bulk composition of the primary pyroxenes, then the Sm-Nd isochron age and ε_{Nd} will be in error. *Copyright © 2002 Elsevier Science Ltd*

1. INTRODUCTION

This article presents detailed results of a secondary ion mass spectrometry (SIMS) study of the minerals of two lunar ferroan anorthosites. The data are a subset of a much larger data set collected as a study of the rare earth element (REE) compositions of the minerals in the subgroups of lunar ferroan anorthosites defined by James et al. (1989). The primary purpose of the study was to investigate the relationships among the ferroan–anorthosite subgroups. An abstract by Floss et al. (1991) presented preliminary results, a Ph.D. thesis by Floss (1991) presented and discussed all individual analyses, and an article by Floss et al. (1998) presented averaged analyses of minerals from samples of all four subgroups and discussed possible relationships among the subgroups.

A secondary purpose of the study was to investigate possible preservation of primary REE compositions in the minerals of two of the samples: one of these is 64435,270, a troctolitic anorthosite in which relict igneous texture is exceptionally well preserved (James et al., 1989), and the other is 60025,699, a recrystallized cataclastic "harzburgite" in which relict texture indicates that the bulk of the pyroxene is inverted pigeonite (James et al., 1991). This article presents this secondary aspect of the study. The data for these two samples elucidate how rare earth elements vary in pyroxenes as a result of processes occurring during igneous crystallization and subsequent subsolidus reequilibration, and these results have application to REE studies of all pyroxenes, no matter what their planet or asteroid of origin.

2. METHODS

REE and other trace-, minor- and major-element analyses were made with a modified Cameca IMS-3f ion microprobe at Washington University, St. Louis, Missouri, according to the

* Author to whom correspondence should be addressed (ojames@usgs.gov).
† Present address: Lockheed Martin Inc., P.O. Box 1072, Schenectady, NY 12301, USA.

methods described by Zinner and Crozaz (1986). Secondary ions were sputtered from the sample surfaces with an O^- primary beam at beam currents from 1 to 10 nA, resulting in spot sizes ranging from 10 to 50 μm. Complex molecular interferences were eliminated by energy filtering at low mass resolving power, and the resulting mass spectrum was deconvolved to remove simple molecular interferences (e.g., $REEO^+$). Because light REE (LREE) monoxides are removed from the masses of the heavy REEs (HREEs), LREE-enriched phases, such as plagioclase, typically have larger errors associated with the HREE concentrations than other phases. For details of the experimental procedures, see Floss et al. (1990). Sensitivity factors for the REEs were determined from standards of known REE concentrations. Synthetic glass standards (Drake and Weill, 1972) were used for pyroxenes and olivine, whereas sensitivity factors determined from lunar anorthite crystals (Floss and Jolliff, 1997) were used for plagioclase. Sensitivity factors for elements other than the REEs are given by Hsu (1995). All analyses were normalized using Si as a reference element and SiO_2 concentrations determined by electron probe microanalysis with an automated ARL-SEMQ electron microprobe (see James et al., 1989, 1991, for analyses and details of the electron-probe analytical procedure). Sample 60025,699 was made from a split previously irradiated for instrumental neutron activation analysis (INAA) (James et al., 1991). Because several of the REE masses measured by the ion probe have large cross sections for the absorption of thermal neutrons, they and their daughter isotopes will have anomalously low and high abundances, respectively. We corrected for this effect using the known neutron flux and the basic equation governing the rate of destruction of an isotope; see Floss et al. (1998) for more details about this correction procedure.

3. TEXTURES, MINERALOGY, AND MINERAL CHEMISTRY OF ANALYZED SAMPLES

The two samples we studied are members of the mafic–magnesian subgroup of lunar ferroan anorthosites. Lunar ferroan anorthosites have been subdivided into four subgroups (James et al., 1989), the most important of which are the anorthositic ferroan and mafic magnesian. Most ferroan anorthosites belong to the anorthositic-ferroan subgroup; mafic minerals make up less than 5 vol% of these rocks, are mostly pyroxenes (both orthopyroxene and augite), and are relatively ferroan (orthopyroxene is En_{55-66}). Only five large hand specimens belong to the mafic–magnesian subgroup. Mafic minerals make up 8 to 20 vol% of these rocks and are relatively magnesian (orthopyroxene is En_{67-75}); in addition to orthopyroxene and augite, olivine is present in all samples and abundant in many. Plagioclases have similar anorthite (An) contents in samples of both subgroups.

3.1. Coarse-Grained Troctolitic Anorthosite 64435,270

This sample was found as a clast in lunar breccia 64435. A chip (64435,239) was subdivided into four splits that were analyzed by INAA. Separate chips of this lithology were made into probe mounts, one of which (64435,270) we analyzed by SIMS. Geologic occurrence, hand specimen description, modes, textures, mineralogy, and INAA analyses were presented by James et al. (1989); a summary is given below.

3.1.1. Mode, Texture, Crystallization Sequence, and Major-Element Mineral Compositions

Major minerals are plagioclase, olivine, and inverted pigeonite. Primary augite is a minor mineral, and a trace amount of orthopyroxene derived by reaction of olivine is present. Because the thin sections are small, the mode is uncertain, but the parent rock apparently contained between 11 and 21 vol% mafic minerals; olivine is the most abundant of these.

Relict igneous texture (Figs. 1a–c) ranges from hypidiomorphic granular to subophitic, and grain sizes are coarse for lunar igneous rocks. Textures indicate the crystallization sequence and subsolidus history. Plagioclase and olivine were the first major minerals to crystallize, and plagioclase crystallized throughout the sequence. Olivine reacted with the melt, forming narrow rims of orthopyroxene (Figs. 1a, b). Subsequently, orthopyroxene ceased crystallizing and pigeonite precipitated, commonly rimming earlier formed olivine, orthopyroxene or both (Fig. 1b). Later, augite and pigeonite coprecipitated (Fig. 1c). After the rock had solidified, the pigeonite inverted to a blebby intergrowth of orthopyroxene and augite (Figs. 1b,c). The rock subsequently experienced two periods of mild shock-induced deformation, the first of which was followed by recrystallization.

Electron probe microanalysis indicates that the minerals show only small variations in major-element compositions. Plagioclase averages $An_{97.0}$ (range, $An_{95.7-98.2}$), and olivine averages $Fo_{71.5}$ (range, $Fo_{71.1-71.9}$). Orthopyroxene averages $Wo_{1.5}En_{74.5}Fs_{24.0}$ (range, $Wo_{1.0-2.0}En_{73.2-76.0}Fs_{22.9-25.0}$) and augite averages $Wo_{45.3}En_{45.6}Fs_{9.1}$ (range, $Wo_{44.0-46.2}$ $En_{44.9-46.4}Fs_{8.1-10.1}$); there are no variations in major-element composition correlated with the mode of formation of the pyroxene.

3.1.2. Textures of Minerals Analyzed by SIMS

The eight SIMS analyses we made (Table 1, Fig. 2) represent the following: primary olivine; orthopyroxene derived by reaction of olivine with melt; orthopyroxene and augite derived by inversion of pigeonite; primary augite cocrystallized with pigeonite; primary plagioclase; and recrystallized plagioclase. The mafic–mineral grains analyzed are shown in Figures 1a–c. The primary augite analyzed (Fig. 1c) contains very fine, closely spaced exsolved lamellae of orthopyroxene and abundant exsolved platelets of oxide minerals, indicating that phase separation during subsolidus reequilibration was on a very fine scale. Calcium content of the analyzed spot ($Wo_{30.7}$) corresponds to that of a primary augite formed at a temperature ~1200°C, according to phase relations calculated by Sack and Ghiorso (1994). Although the very fine exsolution of low-Ca pyroxene indicates that the augite has equilibrated on a fine scale to low temperatures, this exsolution is so fine that the relatively large volume sampled by the ion microprobe beam likely approximates the composition of the primary augite.

3.2. Cataclastic "Harzburgite" 60025,699

Sample 60025 is a cataclastic anorthosite consisting mostly of material derived from parent rocks of the anorthositic–ferroan subgroup but locally containing patches of coarse-grained mafic minerals derived from mafic–magnesian parent

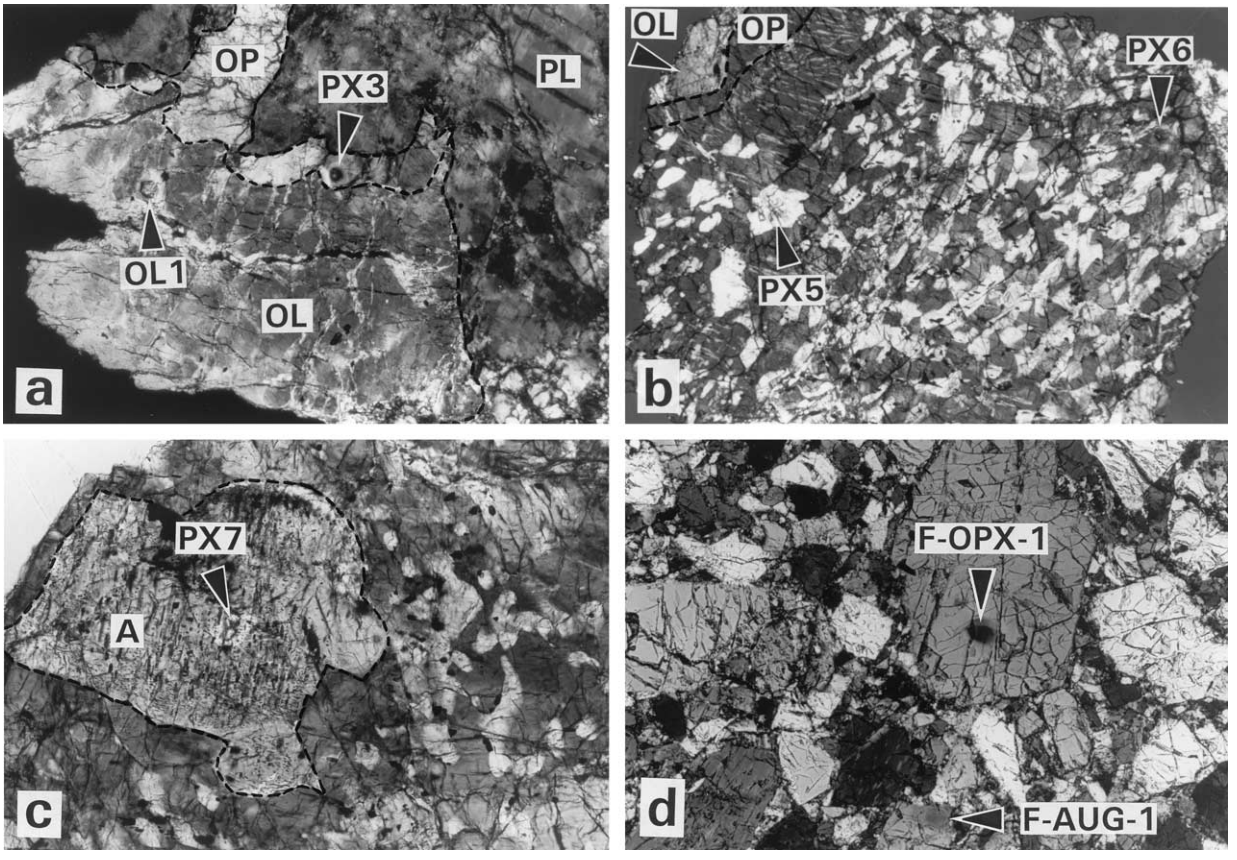

Fig. 1. Photomicrographs of ferroan anorthosites analyzed in this study. (a) Troctolitic anorthosite 64435,270. Olivine (OL) is partly rimmed by reaction-derived orthopyroxene (OP); mineral contacts are marked by dashed lines. Olivine, pyroxene, and plagioclase (PL) show shock-induced fracturing and patchy extinction. Locations of analyzed spots for olivine (OL1) and reaction-derived orthopyroxene (PX3) are indicated by arrows. Field width is 1.41 mm; crossed polarizers. (b) Troctolitic anorthosite 64435,270. Olivine (OL) has a narrow rim of reaction-derived orthopyroxene (OP) and is enclosed by inverted pigeonite, consisting of orthopyroxene (gray) packed with blebs and lenses of augite (white). Contacts between olivine and reaction-derived orthopyroxene and between inverted pigeonite and reaction-derived orthopyroxene are marked by dashed lines. Locations of analyzed spots for inversion-derived orthopyroxene (PX6) and inversion-derived augite (PX5) are indicated by arrows. Field width is 1.75 mm; partly crossed polarizers. (c) Troctolitic anorthosite 64435,270. Primary augite (A) is enclosed by inverted pigeonite (gray orthopyroxene containing blebs of white augite); contact between primary augite and inverted pigeonite is marked by a dashed line. Location of the analyzed spot of primary augite (PX7) is marked by an arrow. Field width is 0.88 mm; partly crossed polarizers. (d) "Harzburgite" 60025,699. Lithic fragment consisting of recrystallized granulated aggregate of olivine, orthopyroxene, and augite; mineral clasts are angular and have seriate size distribution. Locations of analyzed spots for orthopyroxene F-OPX-1 and augite F-AUG-1 are marked by arrows. Field width is 0.88 mm; crossed polarizers.

rocks. The subsample we studied, 60025,699, consisted of two small chips taken from the patches of magnesian mafic minerals. The chips were broken into smaller fragments and subdivided by hand-picking into two splits, which were analyzed by INAA and subsequently made into the two probe mounts we studied, 60025,699SM (60025,9016) and 60025,699LM (60025,9017). Modes, textures, and mineralogy of this sample were described in detail and the INAA analyses were presented by James et al. (1991); a summary is given below.

3.2.1. Mode, Texture, and Major-Element Mineral Compositions

Major minerals are olivine, orthopyroxene, and augite (the latter two were derived mostly by inversion of primary pigeonite), and plagioclase is a minor mineral. Olivine makes up 41 to 45% by volume of the probe mounts, orthopyroxene 45 to 51%, augite 5 to 7%, and plagioclase 1 to 5%. The mode of the parent rock is uncertain because plagioclase was intentionally excluded in sampling.

Both probe mounts studied are grain mounts of lithic and mineral fragments. The lithic fragments are recrystallized olivine–pyroxene cataclasites (Fig. 1d). Relict igneous texture is poorly preserved, but original grain size was apparently coarse. All large pyroxene clasts consist of blebby or lamellar intergrowths of augite and orthopyroxene, indicating they represent inverted pigeonites. The rock experienced two periods of shock-induced deformation after it solidified; the first produced the cataclastic texture, which was followed by the healing of the grain contacts.

Electron-probe microanalysis indicates that the minerals

Table 1. Rare-earth element concentrations (ppm) and wollastonite contents (%) in minerals from troctolitic anorthosite 64435,270[a]

	Orthopyroxene		Augite		Olivine	Plagioclase		
Element	270PX3[C] Reaction-derived	270PX6[B] Inversion-derived	270PX5[B] Inversion-derived	270PX7[A] Primary	270OL1[C] Primary	270PL1[D] Primary	270PL2[C] Primary	270PL3[C] Recrystallized
La	0.009 ± 0.003	0.016 ± 0.004	0.715 ± 0.084	0.644 ± 0.066		0.713 ± 0.083	0.530 ± 0.084	0.496 ± 0.077
Ce	0.027 ± 0.007	0.062 ± 0.014	4.601 ± 0.396	3.559 ± 0.338		1.653 ± 0.177	1.421 ± 0.169	1.321 ± 0.143
Pr	0.007 ± 0.003	0.014 ± 0.004	1.196 ± 0.125	1.040 ± 0.122		0.213 ± 0.032	0.216 ± 0.035	0.189 ± 0.026
Nd	0.067 ± 0.012	0.096 ± 0.014	7.874 ± 0.447	5.658 ± 0.313		0.731 ± 0.066	0.757 ± 0.070	0.683 ± 0.059
Sm	0.084 ± 0.018	0.076 ± 0.016	3.613 ± 0.383	2.801 ± 0.269		0.132 ± 0.030	0.118 ± 0.030	0.153 ± 0.040
Eu		0.004 ± 0.003	0.040 ± 0.024	0.022 ± 0.019		1.012 ± 0.093	0.921 ± 0.087	0.980 ± 0.074
Gd	0.238 ± 0.060	0.243 ± 0.047	6.388 ± 0.767	5.040 ± 0.550		0.117 ± 0.032	0.112 ± 0.037	0.170 ± 0.040
Tb	0.100 ± 0.016	0.089 ± 0.014	1.479 ± 0.184	0.986 ± 0.119	0.002 ± 0.001	0.024 ± 0.008	0.023 ± 0.008	0.022 ± 0.007
Dy	0.916 ± 0.087	0.831 ± 0.079	9.925 ± 0.591	7.098 ± 0.410	0.014 ± 0.004	0.061 ± 0.013	0.101 ± 0.016	0.093 ± 0.013
Ho	0.287 ± 0.038	0.229 ± 0.035	1.938 ± 0.172	1.487 ± 0.176	0.011 ± 0.003	0.019 ± 0.005	0.024 ± 0.006	0.016 ± 0.004
Er	1.218 ± 0.100	1.112 ± 0.097	5.758 ± 0.367	4.695 ± 0.309	0.063 ± 0.008	0.025 ± 0.009	0.049 ± 0.014	0.042 ± 0.011
Tm	0.244 ± 0.036	0.174 ± 0.027	0.736 ± 0.085	0.578 ± 0.075	0.021 ± 0.004			
Yb	1.908 ± 0.152	1.591 ± 0.130	4.275 ± 0.390	3.911 ± 0.367	0.202 ± 0.017	0.041 ± 0.011	0.041 ± 0.013	0.035 ± 0.010
Lu	0.320 ± 0.043	0.287 ± 0.045	0.559 ± 0.128	0.529 ± 0.078	0.059 ± 0.009			
Wo	1.7	1.6	44.8	30.7				

[a] Data from Floss (1991), with plagioclase analyses adjusted using sensitivity factors determined by Floss and Jolliff (1997). Errors are 2σ, from counting statistics; values not listed are below detection limits. Sample designations from Floss et al. (1998) are as follows: A, Clast A; B, Clast B; C, Clast C; and D, Clast D.

mostly show only small variations in major-element compositions. Plagioclase averages $An_{97.9}$ (range, $An_{96.0-98.9}$) and olivine averages $Fo_{65.3}$ (range, $Fo_{64.4-66.0}$). Orthopyroxene averages $Wo_{2.5}En_{69.7}Fs_{27.8}$ (range, $Wo_{1.9-4.1}En_{68.4-71.5}Fs_{26.3-29.1}$) and augite averages $Wo_{45.3}En_{43.7}Fs_{11.0}$ (range, $Wo_{43.8-46.3}En_{42.3-44.9}Fs_{9.9-11.8}$).

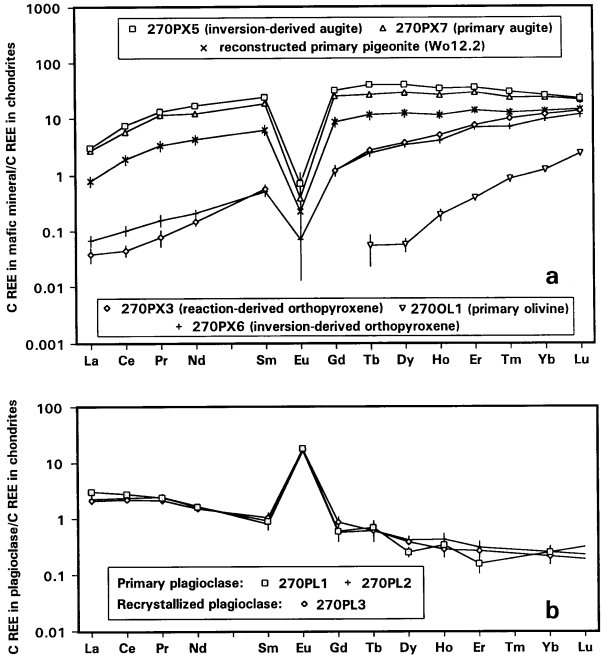

Fig. 2. Chondrite-normalized REE compositions of the minerals in troctolitic anorthosite 64435,270 (chondrite composition used is mean C1 chondrite from Anders and Grevesse, 1989). Error bars (2σ) are shown by vertical lines (for many data points, error bars are smaller than the plotted symbols). Errors for reconstructed pigeonite assume 5% absolute error in mode. (a) Pyroxenes and olivine. (b) Plagioclase.

3.2.2. Textures of Minerals Analyzed by SIMS

Twelve SIMS analyses were made of the minerals in the probe mounts studied (Table 2, Fig. 3). Because these samples consist of recrystallized granulated aggregates and were extensively disaggregated for INAA analysis, the analytical spots cannot be related to primary igneous textures. The Mg#s (100 × molar Mg/[Mg + Fe]) indicate that all of the mafic minerals analyzed are from a mafic–magnesian parent rock. The source of the analyzed plagioclase is uncertain, however, so we do not present any of the analyses herein (see Floss, 1991, and Floss et al., 1998, for the data).

Mafic–mineral grains analyzed in 60025,699SM are an olivine, an orthopyroxene, and two augites. The olivine is a 100-μm angular clast within a lithic fragment, and augite SM-J-AUG1 is a bleb within a 0.6-mm clast of inverted pigeonite in the same lithic fragment. Augite SM-F-AUG2 and the orthopyroxene are clasts separated by 300 μm within a second lithic fragment (Fig. 1d); the orthopyroxene is a 300-μm monomineralic clast, and the augite is in a 90-μm clast of inverted pigeonite.

Mafic–mineral grains analyzed in 60025,699LM are three orthopyroxenes and two augites. Orthopyroxene LM-M-OPX3 is within a fragment of inverted pigeonite. Orthopyroxene LM-G-OPX2 is a 0.5-mm clast within a lithic fragment. Orthopyroxene LM-O-OPX1 and the two augites are angular monomineralic fragments.

3.3. Comparison of SIMS and INAA REE Data

The two splits of 60025,699 studied by SIMS and a bulk-rock split of the 64435 troctolitic anorthosite were analyzed by INAA before being made into probe mounts. Modes were determined on each probe mount by point counting on backscattered electron images made with a scanning electron mi-

Table 2. Rare element concentrations (ppm) and wollastonite contents (%) in mafic minerals from "harzburgite" 60025,699[a]

	Orthopyroxene			Augite		Orthopyroxene	Olivine	Augite	
Element	LM-O-OPX1 Monomineralic	LM-G-OPX2	LM-M-OPX3 Inversion-derived	LM-O-AUG1 Monomineralic	LM-P-AUG2 Monomineralic	SM-F-OPX1	SM-J-OL1	SM-J-AUG1 Inversion-derived	SM-F-AUG2 Inversion-derived
La	0.004 ± 0.002	0.003 ± 0.002	0.003 ± 0.002	0.381 ± 0.061	0.401 ± 0.054			0.268 ± 0.048	0.335 ± 0.048
Ce	0.025 ± 0.005	0.015 ± 0.005	0.024 ± 0.006	1.961 ± 0.195	2.019 ± 0.206	0.013 ± 0.005		1.344 ± 0.219	1.933 ± 0.244
Pr	0.008 ± 0.002	0.004 ± 0.002	0.006 ± 0.002	0.421 ± 0.063	0.492 ± 0.090	0.006 ± 0.003		0.281 ± 0.049	0.484 ± 0.072
Nd	0.074 ± 0.010	0.039 ± 0.009	0.062 ± 0.010	3.260 ± 0.248	3.664 ± 0.266	0.048 ± 0.011		2.144 ± 0.226	3.212 ± 0.258
Sm	0.066 ± 0.012	0.032 ± 0.011	0.061 ± 0.013	1.958 ± 0.242	2.084 ± 0.217	0.051 ± 0.014		1.785 ± 0.264	1.956 ± 0.248
Eu				0.060 ± 0.020	0.055 ± 0.022			0.071 ± 0.023	0.043 ± 0.021
Gd	0.079 ± 0.035	0.072 ± 0.028	0.082 ± 0.024	1.075 ± 0.360	1.318 ± 0.401	0.069 ± 0.028		1.469 ± 0.332	1.132 ± 0.331
Tb	0.049 ± 0.008	0.039 ± 0.008	0.046 ± 0.012	0.432 ± 0.094	0.491 ± 0.108	0.045 ± 0.013		0.462 ± 0.132	0.466 ± 0.089
Dy	0.512 ± 0.050	0.420 ± 0.045	0.473 ± 0.045	3.769 ± 0.313	4.240 ± 0.346	0.471 ± 0.055		3.348 ± 0.328	3.652 ± 0.350
Ho	0.115 ± 0.017	0.115 ± 0.024	0.144 ± 0.024	0.621 ± 0.122	0.760 ± 0.107	0.128 ± 0.028	0.002 ± 0.001	0.597 ± 0.114	0.788 ± 0.111
Er	0.515 ± 0.043	0.517 ± 0.059	0.548 ± 0.053	2.156 ± 0.216	2.267 ± 0.225	0.489 ± 0.062	0.013 ± 0.004	1.765 ± 0.209	1.759 ± 0.183
Tm	0.092 ± 0.016	0.090 ± 0.018	0.088 ± 0.015	0.302 ± 0.051	0.322 ± 0.054	0.095 ± 0.017	0.005 ± 0.002	0.206 ± 0.050	0.295 ± 0.046
Yb	0.830 ± 0.075	0.778 ± 0.091	0.749 ± 0.094	1.962 ± 0.206	2.331 ± 0.225	0.857 ± 0.106	0.056 ± 0.011	1.875 ± 0.213	1.915 ± 0.203
Lu	0.120 ± 0.019	0.132 ± 0.020	0.146 ± 0.035	0.217 ± 0.048	0.269 ± 0.052	0.146 ± 0.036	0.014 ± 0.005	0.132 ± 0.043	0.210 ± 0.060
Wo	2.9	2.4	2.7	42.6	44.4	2.2		43.9	41.1

[a] Data from Floss (1991). Errors are 2σ, from counting statistics; values not listed are below detection limits.

croscope (James et al., 1989, 1991). We used the modes (converted to wt%) and the REE compositions of the minerals determined by SIMS to reconstruct the bulk compositions of the splits. For all three splits, agreement between the INAA analysis and the SIMS modal reconstruction is excellent (Floss et al., 1998).

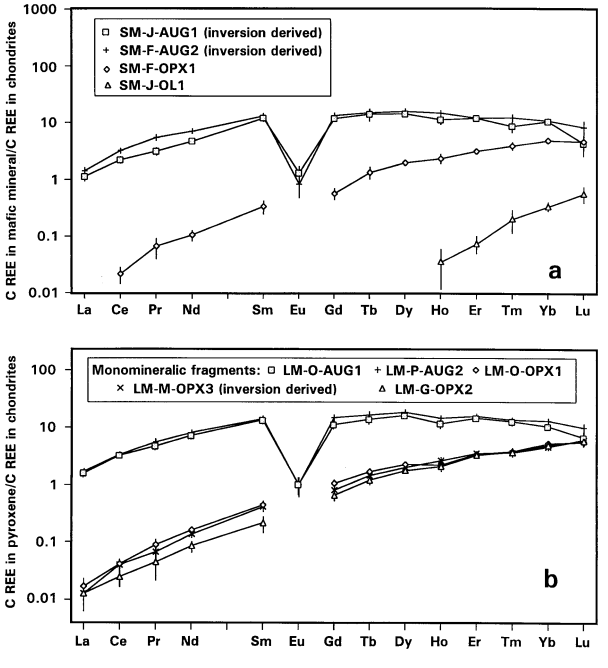

Fig. 3. Chondrite-normalized REE compositions of the mafic minerals in "harzburgite" 60025,699 (chondrite composition used is mean C1 chondrite from Anders and Grevesse, 1989). Error bars (2σ) are shown by vertical lines (for many data points, error bars are smaller than the plotted symbols). (a) Pyroxenes and olivine in 60025,699SM. (b) Pyroxenes in 60025,699LM.

4. RARE EARTH ELEMENT CONTENTS OF MINERALS DETERMINED BY SIMS

4.1. Troctolitic Anorthosite 64435,270

The REE patterns for the minerals we analyzed in 64435,270 are shown in Figure 2, including an estimate of the composition of the primary pigeonite reconstructed from its mode and the SIMS analyses of the inversion products. Point counts performed on a SEM backscattered electron image of the analyzed grain of inverted pigeonite indicate that it consists of 24.3 vol% augite and 75.7 vol% orthopyroxene. Although a mode determined on a random slice through a grain of inverted pigeonite may not give the true proportion of phases because exsolution commonly occurs along crystallographically controlled planes, exsolution in this grain is blebby, and the uniform distribution of augite blebs suggests that the mode probably is close to representative of the true mineral proportions. The reconstructed pigeonite has a composition of $Wo_{12.2}$. According to phase relations calculated by Sack and Ghiorso (1994), the crystallization temperature of such a pigeonite would have been ~1150°C. This temperature corresponds well with that indicated by the composition of the primary augite (1200°C), reinforcing our assumption that the calculated pigeonite bulk composition is close to the true bulk composition. Because we have only one analysis of inversion-derived orthopyroxene and one analysis of inversion-derived augite, we have no information on the homogeneity of these inversion products.

It has long been known that pyroxene REE patterns vary according to mineral structure and Ca content (Schnetzler and Philpotts, 1970; Gromet et al., 1981; McKay et al., 1986; Shearer et al., 1989), and the pyroxenes we analyzed show the predicted differences (Fig. 2a). Orthopyroxenes have low REE abundances and their REE patterns are HREE enriched and relatively straight, whereas the clinopyroxenes (augite and pigeonite) have higher REE abundances and their REE patterns are HREE enriched but convex upward, especially in the LREEs. The REE contents of the clinopyroxenes are positively

correlated with Ca content. The inversion-derived augite, which has a higher Ca content than the primary augite ($Wo_{44.8}$ vs. $Wo_{30.7}$), has higher REE contents; differences are greater than 2σ errors for all elements except La, Pr, Yb, and Lu. Both augites have higher REE abundances than the reconstructed pigeonite ($Wo_{12.2}$).

In this sample, pyroxene REE patterns also vary depending on the mode of formation. Orthopyroxene that formed by reaction of olivine with melt has slightly higher HREE contents and lower LREE contents than orthopyroxene that formed by inversion of pigeonite (differences are greater than 2σ errors for La, Ce, Pr, Nd, Ho, Tm, and Yb). Augite that formed by inversion of pigeonite ($Wo_{44.8}$) is not as enriched in LREEs relative to the primary augite ($Wo_{30.7}$) as would be predicted from the differences in Ca contents between these minerals (compare patterns on Fig. 2a with predicted patterns on Fig. 6a).

The REE patterns of the three plagioclase grains analyzed in this sample (Fig. 2b) are identical within errors. The patterns show LREE enrichment and positive Eu anomalies and are fairly straight. The olivine (Fig. 2a) has very low REE concentrations and a HREE-enriched pattern with a steep slope; only REEs heavier than Gd had abundances above 2σ detection limits.

4.2. Harzburgite 60025,699

In 60025,699SM, the analyzed olivine and pyroxenes have REE patterns (Fig. 3a) similar in shape to those of the same minerals in 64435,270, but the REE abundances are lower. The two augites in 60025,699SM have similar Ca contents ($Wo_{41.1}$ and $Wo_{43.9}$) and differ slightly in LREE contents; differences are greater than 2σ errors for Ce, Pr, and Nd. In the olivine, only REEs heavier than Dy are present in abundances above 2σ detection limits.

In 60025,699LM, the two augites analyzed have similar Ca contents ($Wo_{42.6}$ and $Wo_{44.4}$) and nearly identical REE patterns (Fig. 3b) that are also nearly identical to that of the more REE rich of the two augites in 60025,699SM. The three orthopyroxenes have REE abundances (Fig. 3b) roughly similar to those in the orthopyroxene in 60025,699SM but have REE (especially LREE) abundances that vary slightly; the REE abundances are positively correlated with the Ca contents of the analyzed spots. The differences for all elements in the two higher-Ca orthopyroxenes ($Wo_{2.7}$ and $Wo_{2.9}$) are within 2σ errors. In the lowest-Ca orthopyroxene ($Wo_{2.4}$), Nd and Sm are lower by more than 2σ errors than in the other two orthopyroxenes, and Gd, Tb, and Dy are lower by more than 2σ errors than in the highest-Ca orthopyroxene.

The composition of primary pigeonite in 60025,699 is not as easy to determine as in 64435,270. We could calculate its composition by assuming that all the pyroxene in the rock is derived by inversion of pigeonite, but this calculation would be valid only if there were no primary augite, primary orthopyroxene, or reaction-derived orthopyroxene. Augite makes up only 12% by volume of the bulk pyroxene, and the Ca content this percentage implies for an original pigeonite (Wo_7) seems too low in comparison with the primary pigeonite in 64435,270, suggesting that there may be unidentified primary or reaction-derived orthopyroxene. Because of these uncertainties, we have not estimated the bulk composition of the primary pigeonite.

5. DISCUSSION

5.1. Mineral Compositions

In both samples studied, most of the pyroxene is derived by inversion of pigeonite, but 64435,270, which has well-preserved relict igneous texture, also contains primary augite and orthopyroxene derived by reaction of olivine with melt. Throughout each sample, the pyroxenes show small variations in major-element compositions, and the variations are much smaller than would be expected during primary igneous crystallization; thus, it appears that compositions have been homogenized during inversion of pigeonite and subsequent subsolidus reequilibration. The structural changes that occur upon inversion of pigeonite require extensive internal redistribution of major elements, and comparison of REE contents of the inversion products indicate that the REEs were redistributed as well. Exsolution textures and Ca contents of the pyroxenes indicate reequilibration within grains to temperatures ~800°C (based on theoretical phase relations given in Sack and Ghiorso, 1994). In the primary augite analyzed in 64435,270, the SIMS bulk analysis appears to represent the composition of the primary mineral.

Although REEs have clearly been redistributed within pyroxene grains, contents of these elements have not been completely homogenized between grains. Both augite and orthopyroxene show REE variations that are positively correlated with variations in Ca content (e.g., the orthopyroxenes and augites in sample 60025,699LM; Fig. 3b, Table 2). In addition, both augite and orthopyroxene show variations correlated with mode of formation, as follows: despite having a slightly higher Ca content ($Wo_{1.7}$ vs. $Wo_{1.6}$), orthopyroxene formed by reaction of melt with olivine in 64435,270 has lower LREEs than orthopyroxene formed by inversion of pigeonite; and augite formed by inversion of pigeonite in 64435,270 has lower LREEs than would be expected for magmatic augite with the same Ca content. Unfortunately, we have only one analysis per pyroxene grain, so we have no information on whether or not REE compositions vary within grains.

The plagioclases analyzed within each of the two samples we studied have concentrations of major elements, REEs, and other trace elements that are uniform within errors (Floss et al., 1998). Our analyses are all from the centers of grains, and we have only one analysis per grain; thus, we have no information on whether the grains are zoned and the extent to which individual grains have reequilibrated in the subsolidus.

5.2. Solid–Solid Distribution Coefficients

5.2.1. Solid–Solid Distribution Coefficients Calculated from SIMS Data

Concentration ratios for the REEs in mineral pairs (C_{REE} in mineral A/C_{REE} in mineral B) represent solid–solid distribution coefficients if the minerals in the pair were in equilibrium with each other in the subsolidus. Figure 4a shows concentration ratios (C_{REE} in orthopyroxene/C_{REE} in augite) that represent solid–solid Ds for pyroxene pairs that we analyzed (values for

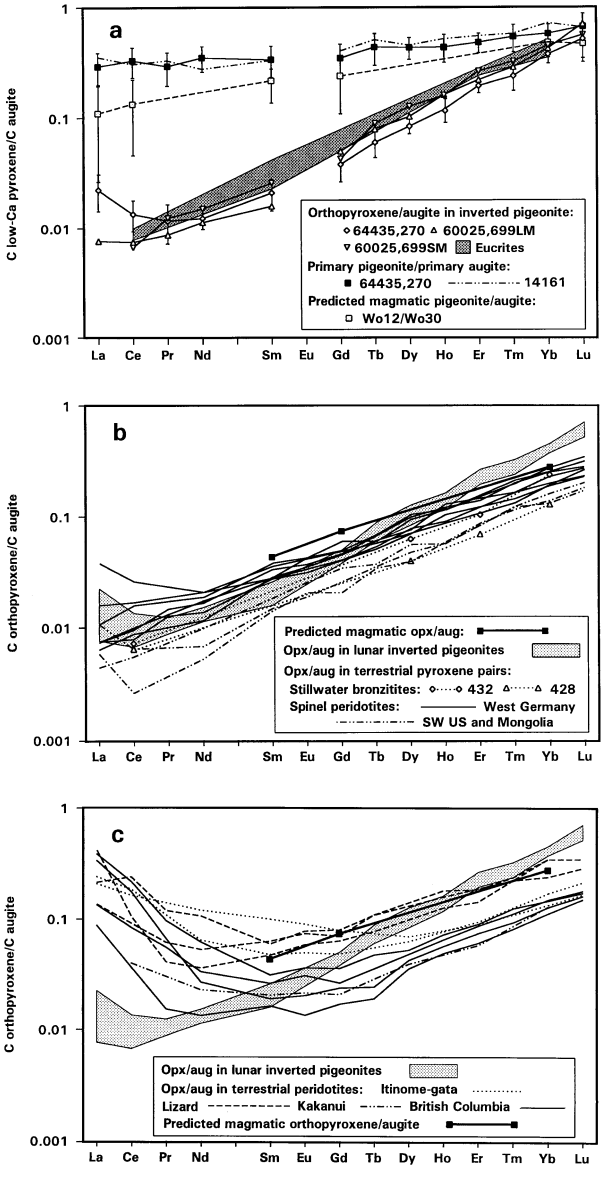

Fig. 4. Concentration ratios and solid–solid distribution coefficients (C_{REE} in low-Ca pyroxene/C_{REE} in augite) for pyroxene pairs. (a) Solid–solid Ds from our data compared with solid–solid Ds for eucritic pyroxene pairs (Pun and Papike, 1995) and concentration ratios for magmatic pyroxene pairs. Errors (2σ) are shown by vertical lines for inversion-derived and primary pyroxene pairs from 64435,270; the error in the mode of reconstructed pigeonite is assumed to be 5% absolute. Solid–solid Ds plotted for eucritic pyroxenes (shaded field) are for orthopyroxene–augite pairs derived by inversion of pigeonite. Predicted concentration ratios for the magmatic pyroxene pair Wo_{12}/Wo_{30} (dashed line) are derived from experimentally determined solid–liquid Ds ($D_{orthopyroxene/augite} = D_{orthopyroxene/liquid}/D_{augite/liquid}$) from McKay et al. (1986); errors are shown for this pyroxene pair. Also shown for comparison are concentration ratios from a Wo_{13}/Wo_{33} primary pigeonite/primary augite pair (dot-dash line) in lunar sample 14161,7373 (Jolliff et al., 1999). (b) Solid–solid Ds for terrestrial pyroxene pairs compared with our solid–solid Ds for lunar pyroxene pairs derived by pigeonite inversion (shaded field). Data for orthopyroxene–augite pairs from terrestrial spinel peridotites are from Stosch (1982); samples are xenoliths from West Germany (Ib/8, Ib/24, Ib/K1, D-42, D-45, D-50, D-58), the southwestern United States (SC-K2, KH-K8) and Mongolia (Mo22), and the minerals were analyzed by radiochemical neutron activation analysis. Data for orthopyroxene–augite pairs from Stillwater bronzitites (Mountain View transect) are from Papike et al. (1995); minerals were analyzed by SIMS. The West German spinel peridotites (solid lines) equilibrated at higher temperature (~1150°C) than other samples (dotted and dot-dash lines; ~1050 to 800°C). Also shown are predicted HREE concentration ratios for a magmatic orthopyroxene/augite pair, where solid–liquid Ds used for orthopyroxene are those for Wo_5 pigeonite (McKay et al., 1991) and solid–liquid Ds used for augite are those for Wo_{42} (McKay et al., 1986). (c) Solid–solid Ds for terrestrial pyroxene pairs compared with our solid–solid Ds for lunar pyroxene pairs derived by pigeonite inversion (shaded field). Terrestrial data are as follows: isotope dilution data for lherzolite inclusions from andesite at Itinome-gata, Japan (Tanaka and Aoki, 1981); inductively coupled plasma mass spectrometry data for lherzolite and olivine websterite nodules from basalt from British Columbia (Sun and Kerrich, 1995); INAA data for lherzolite from the Lizard alpine peridotite body, Cornwall, England (Frey, 1970); and isotope dilution data for a lherzolite nodule from Kakanui, New Zealand (Philpotts et al., 1972). Also shown are predicted HREE concentration ratios for a magmatic orthopyroxene/augite pair (see b above).

Eu are not plotted; they are not reliable because this element is present in such low concentrations in orthopyroxene). The three pyroxene pairs whose concentration ratios represent solid–solid Ds are inversion products of primary pigeonites, reequilibrated to temperatures below the solidus. The pyroxene pair from 64435,270 consists of the orthopyroxene (270PX6) and augite (270PX5) derived from inversion of the same pigeonite grain. Textures clearly indicate that these two minerals are derived by inversion of the same initial pigeonite, and their Ca contents ($Wo_{1.6}/Wo_{44.8}$) suggest that the temperature of reequilibration was ~800°C (Sack and Ghiorso, 1994).

The other two pairs of inversion-derived pyroxenes are in 60025,699. In this rock, textures indicate that all the larger grains of pyroxene are inverted pigeonites, so we will assume that all our analyzed pyroxenes are inversion derived even though most of them are so small that there is no textural evidence for this origin. The pyroxene pair from 60025,699SM consists of orthopyroxene (SM-F-OPX1) and augite (SM-F-AUG2) clasts from the same lithic fragment of olivine–pyroxene cataclasite; these two grains are only 300 μm apart, so it is likely that they would have equilibrated with each other during recrystallization. The Ca contents of these pyroxenes ($Wo_{2.2}/Wo_{41.1}$) suggest an equilibration temperature in the range 800 to 950°C (Sack and Ghiorso, 1994). The pyroxene pair from 60025,699LM consists of the lowest Ca orthopyroxene (LM-G-OPX2) and the highest Ca augite (LM-P-AUG2) in this probe mount; this pairing assumes that all the pyroxene in the sample has reequilibrated and the minerals with the most extreme Ca contents are those that have equilibrated to the lowest temperature. The Ca contents in these pyroxenes ($Wo_{2.4}/Wo_{44.4}$) suggest an equilibration temperature of ~800°C (Sack and Ghiorso, 1994).

All the REE patterns of solid–solid Ds for inversion products of pigeonite (Fig. 4a) are close to straight lines for the REEs Sm-Lu; the most reliable of the patterns, that for 64435,270, turns upward for REEs lighter than Nd (this pattern is the most reliable because it is based on pyroxenes that have relatively high REE concentrations). The Ds agree quite well with solid–solid Ds determined for inversion-derived orthopyroxene–augite pairs in the eucrites Binda ($Wo_{2.2}/Wo_{44.4}$), Moama ($Wo_{2.9}/Wo_{41.6}$), and Serra de Magé ($Wo_{1.8}/Wo_{44.0}$) (Fig. 4a; Pun and Papike, 1995).

Also plotted on Figure 4a are the concentration ratios for the pyroxene pair consisting of the primary augite (270PX7) and the reconstructed primary pigeonite in 64435,270. The Ca contents of these pyroxenes ($Wo_{12.2}/Wo_{30.7}$) suggest a crystallization temperature ~1200°C (Sack and Ghiorso, 1994). The concentration ratios are higher, and their REE pattern has a shallower positive slope than for the pairs derived by pigeonite inversion. Unfortunately, we cannot be certain that these two primary pyroxenes were in equilibrium with each other. In 64435,270, pigeonite began crystallizing before augite, and the analyzed pigeonite inversion products and primary augite are in different chips of the parent rock. If the augite crystallized later than the pigeonite, it might have been in equilibrium with a liquid richer in REEs, especially LREEs. If so, the pigeonite/augite concentration ratios measured herein are lower limits to the actual pigeonite/augite concentration ratios for minerals in equilibrium with the same liquid. However, concentration ratios for a similar primary pyroxene pair ($Wo_{13.3}/Wo_{33.3}$; see Fig. 4a) from lunar sample 14161,7373 (Jolliff et al., 1999) are within error of the concentration ratios for the primary pyroxene pair from 64435,270; this correspondence reinforces our interpretation that the concentration ratios we measured are close to the actual concentration ratios for minerals in equilibrium with the same liquid.

We have also calculated concentration ratios for plagioclase–pyroxene mineral pairs (C_{REE} in plagioclase/C_{REE} in pyroxene) in troctolitic anorthosite 64435,270 (Fig. 5a). We cannot be certain that these values represent distribution coefficients because we cannot be certain that the analyzed plagioclases and pyroxenes were in equilibrium with each other or with the same liquid; the plagioclase composition used is the average of the analyses from this sample.

5.2.2. *Comparison of Measured and Predicted Concentration Ratios and Solid–Solid Distribution Coefficients*

Experimentally determined or measured solid–liquid Ds can be used to derive the concentration ratios that would be expected in the case of mineral pairs in equilibrium with the same magma (for example, $D_{orthopyroxene/augite} = D_{orthopyroxene/liquid}/D_{augite/liquid}$). Experimentally determined and measured solid–liquid Ds for the trivalent REEs are given in Table 3, and the solid–liquid Ds for pyroxenes are plotted in Figure 6a (Ds for divalent Eu are not considered because they are very low in pyroxenes and there are considerable uncertainties in their values).

For the clinopyroxenes pigeonite and augite, data for solid–liquid Ds plotted on Figure 6 are from McKay et al. (1986) and McKay et al. (1991). The McKay et al. (1986) data are for pyroxenes in equilibrium with a shergottite melt, and the McKay et al. (1991) data are for pyroxene in equilibrium with a lunar-basalt melt. Though these melts differ greatly in oxygen fugacity, the Ds for Wo_5 pigeonite from both data sets are fairly similar, suggesting that differences in oxygen fugacity do not have strong effects on Ds for trivalent REEs in pyroxene. All patterns of solid–liquid Ds for the clinopyroxenes are convex upward. The McKay et al. (1986) data clearly demonstrate that REE abundance in clinopyroxene is positively correlated with Ca content. This data set further suggests that slopes of the D patterns steepen with decreasing Ca content and also shows D patterns that are kinked upward at Nd for the pigeonites having the lowest Ca contents. The McKay et al. (1991) data set for Wo_5 pigeonite differs from the 1986 data set in that the D pattern is smoother, not as steep, less strongly convex upward, and not kinked upward at Nd. Because the McKay et al. (1986) data set is the only one that defines variations in Ds with variations in Ca content, we use it here. Our data, however, suggest that both the 1986 and 1991 pigeonite experiments may have underestimated all Ds, especially for La and Ce, so that the true patterns may be higher and not as steep as shown in Figure 6a (see Fig. 8).

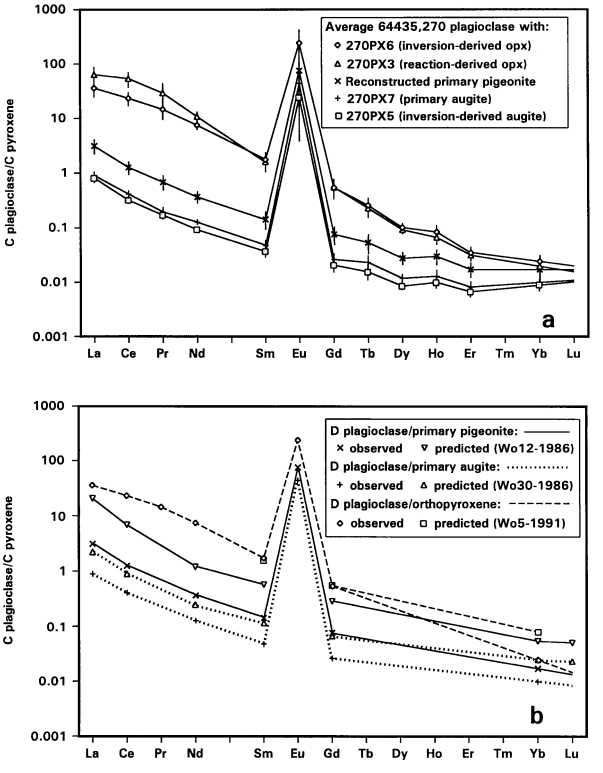

Fig. 5. Concentration ratios for REEs in plagioclase–pyroxene pairs (C_{REE} in plagioclase/C_{REE} in pyroxene) in troctolitic anorthosite 64435,270. (a) REE concentration ratios from our SIMS data. Errors (2σ) are shown by vertical lines; the error in the mode of reconstructed pigeonite is assumed to be 5% absolute. (b) Our measured REE concentration ratios for plagioclase with primary pyroxenes and with inversion-derived orthopyroxene, compared with predicted magmatic concentration ratios for plagioclase–pyroxene pairs in equilibrium with the same liquid. The predicted patterns are derived from solid–liquid Ds listed in Table 3.

For orthopyroxene, determination of solid–liquid Ds has proved very difficult because of the low REE abundances in this mineral. Experimentally determined and measured solid–liquid Ds (Weill and McKay, 1975; Colson et al., 1988; Schnetzler and Philpotts, 1970) vary by nearly two orders of magnitude, but slope of the patterns for the HREE Ds is similar for all determinations. In this study, we use solid–liquid Ds determined by McKay et al. (1991) for HREEs in Wo_5 pigeonite as solid–liquid Ds for HREEs in orthopyroxene. We have made this selection because the Ds are at appropriate values relative to other Ds; and because the slope of the pattern of Ds is appropriate, as indicated by the experimental studies of or-

Table 3. Measured and experimentally determined solid–liquid distribution coefficients

		Pigeonite							Plagioclase		Augite				
Element	Orthopyroxene[a]	Wo_{12}[b]	Wo_3[c]	Wo_5[c]	Wo_5[d]	Wo_{12}[c]	Wo_{16}[c]	Error[c]		Error	Wo_{30}[c]	Wo_{32}[c]	Wo_{36}[c]	Wo_{42}[c]	Error[c]
La		0.00540	0.00052	0.0007		0.00203	0.00374	50%	0.0415[e]	12%	0.0187	0.02263	0.03322	0.0591	26%
Ce	0.009	0.01087	0.00121	0.00161	0.00172	0.00439	0.0078	50%	0.0297[e]	13%	0.0332	0.0389	0.0533	0.0856	15%
Nd		0.03270	0.00606	0.00785	0.0058	0.01944	0.0326	44%	0.023[f]	10%	0.0942	0.1037	0.1255	0.1674	12%
Sm	0.022	0.0515	0.00795	0.01078	0.011	0.03127	0.0575	22%	0.0177[e]	9%	0.1542	0.1673	0.1971	0.2521	12%
Gd		0.0629	0.01227	0.01618	0.021	0.04256	0.074	44%	0.012[f]	10%	0.1825	0.1963	0.227	0.2825	10%
Tb									0.0096[e]	11%					
Dy									0.009[f]	20%					
Ho									0.0084[f]	20%					
Er									0.0079[f]	30%					
Yb	0.17	0.1624	0.0679	0.0787	0.087	0.1318	0.177	15%	0.007[e]	36%	0.2832	0.2884	0.2992	0.316	10%
Lu		0.1939	0.0671	0.078		0.1324	0.1792	15%	0.0067[e]	45%	0.2905	0.296	0.3072	0.325	10%

[a] Weill and McKay (1975).
[b] This study.
[c] McKay et al. (1986).
[d] McKay et al. (1991).
[e] Table 2, column B, Phinney and Morrison (1990), errors are 1σ.
[f] Extrapolated from Phinney and Morrison (1990); errors assumed are consistent with those for measured elements.

thopyroxene. We have not selected any Ds for LREEs in orthopyroxene, however. We do not use the McKay et al. (1991) pigeonite LREE Ds because the shape of the pattern is not the same as found in studies of orthopyroxene Ds: patterns of measured and experimentally determined Ds for LREEs in orthopyroxene are relatively straight extensions of the HREE patterns (Schnetzler and Philpotts, 1970; Weill and McKay, 1975) or turn upward (Schnetzler and Philpotts, 1970; Colson et al., 1988), but the pattern for LREE Ds found by McKay et al. (1991) turns downward.

From the experimental solid–liquid Ds, we have calculated predicted concentration ratios (Fig. 6b) for minerals in equilibrium with the same liquid (herein referred to as magmatic concentration ratios); wollastonite contents of the pyroxenes in the hypothetical equilibrium pairs are those predicted by theoretical pyroxene phase relations (Sack and Ghiorso, 1994). We assume that the pattern of HREE concentration ratios for the pair Wo_5 pigeonite-Wo_{42} augite (solid–liquid Ds for pigeonite from McKay et al., 1991) is appropriate for orthopyroxene/augite magmatic HREE concentration ratios.

Predicted magmatic concentration ratios for plagioclase/pyroxene pairs are presented in Figure 6c; the same Ds for plagioclase/liquid (Table 3) are used to calculate all the concentration ratios because the slight variation observed in the plagioclase compositions would not be expected to have produced significant variations in the solid–liquid Ds. All patterns are slightly convex downward. The predicted concentration ratios depend strongly on the Ca content of the pyroxene in equilibrium with the plagioclase. As Ca contents of the pyroxenes increase, their REE contents and solid–liquid Ds increase and the concentration ratios decrease.

Observed and predicted magmatic concentration ratios for low-Ca pyroxene/augite pairs are compared in Figure 4a (the predicted magmatic concentration ratio for Nd is not plotted so that the pattern will be smoother). Only the patterns for primary pigeonite/primary augite pairs are similar to the predicted magmatic patterns; the observed and predicted patterns are within error for all REEs except La and Ce. (It should be noted that, as discussed above, the concentration ratios for primary pigeonite/primary augite are only lower limits to the true magmatic concentration ratios because of the possibility that the augite crystallized slightly later than the pigeonite and was thus in equilibrium with a slightly more REE-enriched liquid.) The concentration ratios (which represent solid–solid Ds) for the pyroxene pairs derived from inversion of pigeonite are much lower than the concentration ratios for magmatic pairs, and their patterns have much steeper positive slopes.

Observed and predicted magmatic concentration ratios for plagioclase/pyroxene pairs in 64435,270 are compared in Figure 5b. The observed patterns for plagioclase/primary pigeonite and plagioclase/primary augite are nearly parallel to the predicted magmatic patterns, but the values are lower. The pattern for plagioclase/inversion-derived orthopyroxene is steeper than the predicted pattern for plagioclase/primary orthopyroxene (where the Ds used for orthopyroxene are those for HREEs in Wo_5 pigeonite determined by McKay et al., 1991).

5.2.3. *Predicted REE Distributions among Pyroxenes*

Many of the relationships among the REE patterns for the pyroxenes and pyroxene concentration ratios can be predicted from crystal-chemical considerations (Gromet et al., 1981; Papike et al., 1988; Shearer et al., 1989). In pyroxenes, the REEs occupy the M2 structural site. In orthopyroxene, this site is relatively small and cannot easily accommodate ions larger than Mn^{2+} (Cameron and Papike, 1981), and the structure is relatively rigid. In augite and pigeonite, however, the M2 site can accommodate a much greater range of ion sizes, from the small Mg^{2+} ions to the large Na^{+} ions, and the structures are less rigid; the capacity to incorporate larger ions is proportional to the Ca content of the pyroxene because the large Ca ions prop open the structure (Gromet et al., 1981; Papike et al., 1988; McKay, 1989; Shearer et al., 1989). Thus, because the REE ions decrease in size systematically from the LREEs to the HREEs, the latter are more easily accommodated in all pyroxenes than the former; furthermore, because of differences in

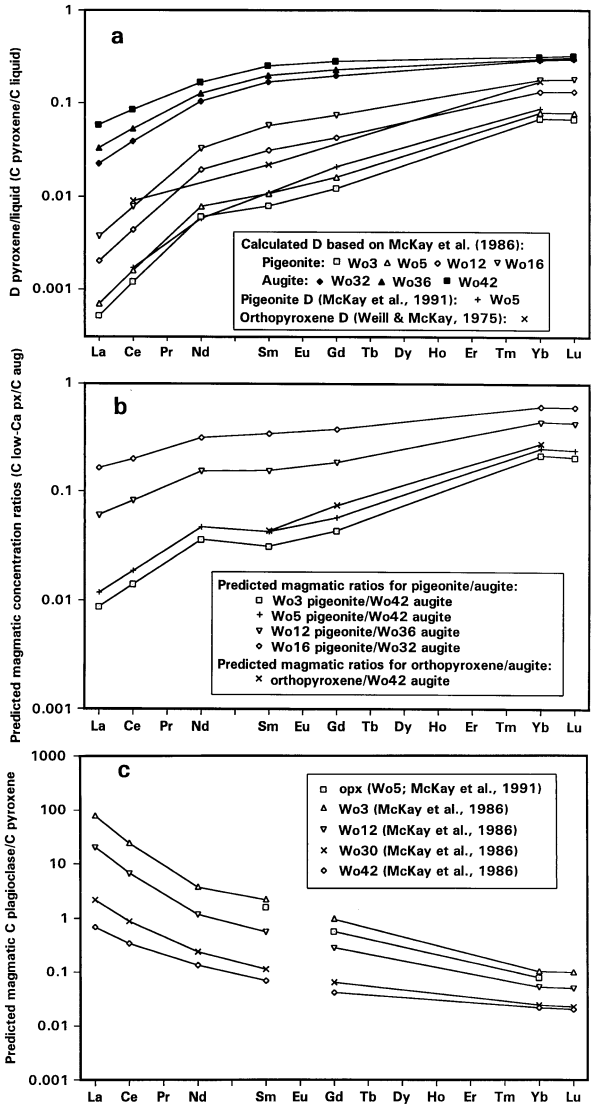

Fig. 6. Experimentally determined solid–liquid Ds for REEs in pyroxenes and predicted concentration ratios for minerals in equilibrium with the same liquid ("magmatic concentration ratios") derived therefrom. (a) Experimentally determined solid–liquid Ds for pyroxenes, from Table 3. Ds for all augites and most pigeonites were determined by equations given in McKay et al. (1986). One set of Ds for Wo_5 pigeonite is from McKay et al. (1991), and Ds for orthopyroxene are from Weill and McKay (1975). (b) Predicted magmatic concentration ratios for pyroxene pairs, calculated from data shown in a. Solid–liquid Ds for pigeonite and augite are from McKay et al. (1986). Solid–liquid Ds for HREEs in orthopyroxene are those for HREEs in Wo_5 pigeonite (McKay et al., 1991). (c) Predicted magmatic concentration ratios for plagioclase–pyroxene pairs.

Ca contents, high-Ca pyroxene can accommodate more REEs than low-Ca pyroxenes. In augite, the amount of Ca in the M2 site enlarges this site to the point that the HREEs are accepted without much relative discrimination (Gromet et al., 1981) and HREE patterns are nearly flat; the patterns turn downward for the LREEs, however, indicating that the larger (and lighter) the LREE, the more it is excluded from the structure. In pigeonite, the M2 site is smaller, the HREEs are less easily accepted, and contents decrease systematically from the heaviest to the lightest ions. In orthopyroxene, the M2 site is even smaller, the REEs are even less easily accepted, and all REE contents decrease from the heaviest to the lightest.

The relative capacities of augite and orthopyroxene to accommodate REEs suggest that, during inversion of pigeonite and subsolidus reequilibration between augite and orthopyroxene, there should be a migration of REEs (especially LREEs) from the orthopyroxene to the augite. This predicted migration of REEs during inversion and subsolidus reequilibration permits prediction of the changes that should take place in solid–solid Ds. As inversion and reequilibration proceed, the solid–solid Ds for orthopyroxene/augite should progressively decrease for all REEs as these elements move from orthopyroxene to augite, and the decrease should be greatest for the LREEs. Accordingly, patterns of solid–solid Ds for pyroxene pairs equilibrated to lower temperatures should be lower and have steeper positive slopes than patterns of solid–solid Ds for pyroxene pairs equilibrated to higher temperatures. These predictions are confirmed by the patterns shown in Figure 4a. The patterns of solid–solid Ds for pyroxene pairs in inverted pigeonites, both lunar and eucritic, are lower and have steeper positive slopes than the patterns of concentration ratios for lunar primary pigeonite/primary augite pyroxene pairs (Fig. 4a); the equilibration temperature of the primary pyroxene pair in 64435,270 is estimated at ~1200°C, whereas equilibration temperatures of the lunar inversion-derived pyroxene pairs are around 800°C.

5.2.4. Differences in Solid–Solid Ds between Extraterrestrial and Terrestrial Pyroxene Pairs

In Figures 4b and 4c, the solid–solid Ds for the lunar inversion-derived pyroxene pairs are compared with solid–solid Ds for orthopyroxene/augite and orthopyroxene/diopside pairs from terrestrial peridotites and Stillwater bronzitites. Solid–solid Ds for terrestrial pyroxene pairs have patterns that vary from fairly straight (Fig. 4b) to strongly convex downward (Fig. 4c). The shapes of these patterns can be predicted from the shapes of the patterns of the analyzed minerals. For most of the pyroxene pairs in samples from the Stillwater complex, West Germany, the southwestern United States, and Mongolia (Fig. 4b), both the orthopyroxene and high-Ca pyroxene show REE patterns of similar shapes but different slopes, the orthopyroxene pattern having a much steeper positive slope. For pairs of this sort, the pattern of solid–solid Ds is close to a straight line. For all of the terrestrial pyroxene pairs whose data are plotted in Figure 4c, the high-Ca pyroxene patterns are strongly convex upward and the orthopyroxene patterns are much straighter, ranging from slightly convex upward to slightly convex downward. For pairs of this sort, the pattern of solid–solid Ds turns upward for the LREEs.

A similar dependence of the shape of the concentration-ratio pattern on the shapes of the mineral patterns can be seen in our data for 64435,270. The primary augite and reconstructed primary pigeonite have REE patterns that are convex upward and similarly shaped (Fig. 2a), so the pattern of concentration ratios for this pair is close to a straight line (Fig. 4a). The inversion-derived augite also has a REE pattern that is convex upward, but the inversion-derived orthopyroxene has a REE pattern that is slightly convex upward for the HREEs but nearly straight for

the LREEs (Fig. 2a); accordingly, the pattern of the solid–solid Ds is close to a straight line for the HREEs but turns upward for the LREEs (Fig. 4a).

At this point, it should be noted that some previous authors have assumed that the patterns of solid–solid Ds for pyroxenes should be straight lines and accordingly they attribute upturns in the LREEs in such patterns to LREE contamination of orthopyroxene. In cases where the REE patterns of the orthopyroxene clearly show LREE enrichment, this interpretation is probably correct, but in the general case, there is no reason to expect that these patterns will be straight lines. The pattern of solid–solid Ds will be a straight line only if the low-Ca and high-Ca pyroxenes have similarly shaped patterns; but if the low-Ca pyroxene pattern is straight and the high-Ca pyroxene pattern is convex upward, the pattern of solid–solid Ds must be convex downward.

The patterns of solid–solid Ds for lunar and eucritic pyroxene pairs are steeper than the patterns for pyroxene pairs from terrestrial rocks (Fig. 4). The observed differences are probably attributable to the fact that the terrestrial pyroxene pairs were in equilibrium with liquid (either during magmatic crystallization or partial melting), whereas the lunar and eucritic pyroxene pairs represent inverted pigeonites and the inversion products were never in equilibrium with liquid. Figures 4b and 4c show a pattern of predicted HREE concentration ratios in a magmatic orthopyroxene/augite pair, where solid–liquid Ds for HREEs in Wo_5 pigeonite (McKay et al., 1991) are used for orthopyroxene and solid–liquid Ds for Wo_{42} augite (McKay et al., 1986) are used for augite. The observed patterns for HREEs in terrestrial pyroxene pairs are parallel to, or slightly steeper than the predicted magmatic pattern, and most of the terrestrial patterns are lower than the predicted magmatic pattern. These relations are consistent with the terrestrial pyroxene pairs having equilibrated with liquid and subsequently having reequilibrated with each other in the subsolidus. During subsolidus reequilibration, the REEs, and especially the LREEs, would have migrated from the orthopyroxene to the high-Ca pyroxene, so that the pattern of solid–solid Ds would be expected to have dropped and steepened with reequilibration to lower temperatures (see section 5.2.3). The data for spinel peridotites from West Germany, the southwestern US and Mongolia (Fig. 4b) show this effect clearly, as pointed out by Stosch (1982): the peridotites from West Germany equilibrated at higher temperature (~1150°C) than the peridotites from the southwestern US (~1050°C), and the latter have patterns that are lower and slightly steeper than the former.

5.2.5. REE Distribution between Plagioclase and Pyroxene

Concentration ratios for the plagioclase–pyroxene pairs in 64435,270 are shown in Figure 5. The observed patterns of concentration ratios for plagioclase/primary pigeonite and plagioclase/primary augite are nearly parallel to the predicted magmatic patterns (Fig. 5b), but the predicted patterns are uniformly higher. These discrepancies indicate that the plagioclase is poorer, or the pyroxenes are richer in REEs than would be predicted for mineral pairs in equilibrium with the same magma (if the solid–liquid Ds for all phases are valid). These discrepancies are discussed in greater detail below.

The observation that the patterns of predicted and observed concentration ratios plotted in Figure 5b are parallel suggests that there has been little or no subsolidus exchange of REEs between the plagioclase and the pyroxenes. If there had been subsolidus exchange, we would expect that the LREEs would have migrated from the pyroxenes to the plagioclase, the HREEs would have migrated from the plagioclase to the pyroxenes, and the observed patterns would have greater negative slopes than the predicted patterns.

Unlike the observed patterns for plagioclase/primary pyroxene pairs, the observed pattern for plagioclase/inversion-derived orthopyroxene (Fig. 5b) has a much steeper negative slope than the predicted magmatic pattern. Floss et al. (1998) discussed the possibility that this discrepancy is due to homogenization within, but not between, minerals and found that this process should produce flatter, not steeper, patterns. The pattern can also be steepened, however, by pigeonite inversion and subsolidus reequilibration between pyroxenes without any exchange with plagioclase. As demonstrated below, the inversion-derived orthopyroxene has a REE pattern with a steeper positive slope than primary orthopyroxene that would have crystallized from the same parent magma. As a result, the pattern of REE concentration ratios for the plagioclase/inversion-derived orthopyroxene pair will have a pattern with a steeper negative slope than the pattern of predicted magmatic concentration ratios.

5.3. Calculated Equilibrium Liquids for Primary, Inverted, and Reacted Minerals

The calculated REE compositions of liquids in equilibrium with the phases analyzed in troctolitic anorthosite 64435,270 are presented in Figure 7; solid–liquid Ds used to calculate these compositions are those given in Table 3. Error bands for equilibrium liquids for the primary minerals are shown in Figure 7b. The REE patterns of equilibrium liquids for all primary minerals are slightly LREE enriched (Fig. 7a). The equilibrium liquid for primary pigeonite is overall richer in REEs than the equilibrium liquid for primary augite and its pattern has a slightly steeper negative slope, but differences are within error for all REEs (Fig. 7b). The equilibrium liquid calculated for plagioclase shows a REE pattern that is roughly parallel to those of the primary pyroxenes, but the liquid is poorer in REEs overall (the difference is greater than error for all REEs except Tb). Compositions of liquids in equilibrium with the phases in "harzburgite" 60025,699 have not been calculated because of uncertainties in the composition of the primary pigeonite and uncertainty concerning which, if any, of the analyzed plagioclases might be from the same parent rock as the pyroxenes.

The "liquids" calculated from the compositions of inversion-derived orthopyroxene and augite (Figs. 7c, d) are depleted in LREEs relative to the equilibrium liquids calculated from the compositions of the primary pyroxenes. The "liquid" calculated from the composition of the inversion-derived augite (Fig. 7c) has heavy REEs like those in the equilibrium liquid for the primary augite but is slightly depleted in LREEs. The "liquids" calculated from the compositions of the inversion-derived and reaction-derived orthopyroxenes (Fig. 7d), using Ds for Wo_5 pigeonite (McKay et al., 1991) as orthopyroxene Ds, are HREE enriched rather than LREE enriched.

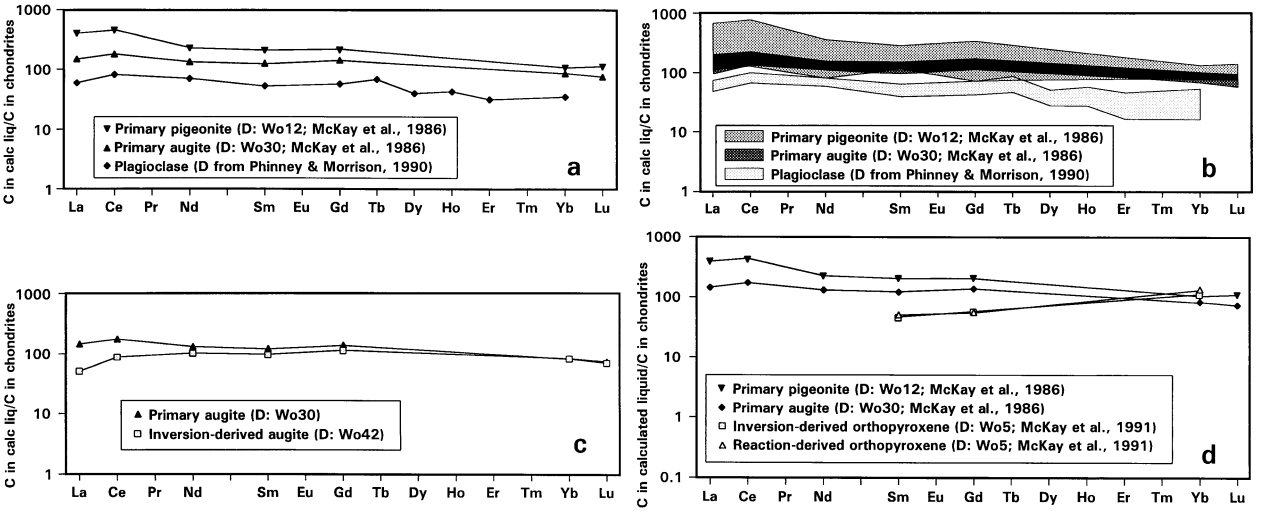

Fig. 7. Chondrite-normalized calculated REE compositions of liquids in equilibrium with primary, inversion-derived, and reaction-derived minerals in troctolitic anorthosite 64435,270 (chondrite composition used is mean C1 chondrite from Anders and Grevesse, 1989). Solid–liquid Ds used to calculate these compositions are given in Table 3. (a) Calculated liquids in equilibrium with primary plagioclase, primary augite, and reconstructed primary pigeonite. (b) Error bands for the equilibrium liquid compositions shown in a, calculated using errors listed in Tables 1 and 3; errors for the composition of reconstructed pigeonite assume 5% absolute error in mode. The band with the darkest shading is the band of overlap of the error bands for primary pigeonite and primary augite. (c) Calculated liquids in equilibrium with primary and inversion-derived augite. (d) Calculated liquids in equilibrium with primary pigeonite, primary augite, inversion-derived orthopyroxene, and reaction-derived orthopyroxene.

5.3.1. REEs in Equilibrium Liquids Calculated from Pyroxene Compositions

The compositional discrepancies between the equilibrium liquids calculated for the primary pyroxenes and for inversion-derived pyroxenes probably arise because the inversion products were never in equilibrium with liquid; thus, the use of solid–liquid Ds to calculate equilibrium-liquid compositions is inappropriate. The LREE depletion of these "equilibrium liquids" indicates that the inversion-derived pyroxenes are depleted in LREEs in comparison to the pyroxenes that would have precipitated directly from liquid. The LREE depletion of the calculated "liquids" is probably a relic of the derivation of these minerals from an original pigeonite; because the primary mineral was LREE depleted relative to its equilibrium liquid, mass balance requires that its inversion products also be LREE depleted relative to the compositions they would have had if they had precipitated from liquid. The LREE depletion of the "liquids" calculated for the reaction-derived orthopyroxene (Fig. 7d) is probably similarly a relic of the derivation of this mineral from a preexisting olivine, which would have been even more strongly LREE depleted than a pigeonite.

These results demonstrate that if one attempts to calculate the compositions of equilibrium liquids from pyroxenes derived by inversion of primary pigeonite or reaction of primary olivine by using experimentally determined solid–liquid Ds for the pyroxenes, the results will be significantly in error. Before calculating the composition of an equilibrium liquid from the composition of an augite or orthopyroxene, it is necessary to determine whether or not the pyroxene is truly primary.

5.3.2. REEs in Equilibrium Liquids Calculated for Primary Phases

Equilibrium liquids calculated from the compositions of analyzed plagioclases have lower REEs than equilibrium liquids calculated from the compositions of analyzed primary pyroxenes (Figs. 7a, b). The same discrepancy is shown in a different way in Figure 5b and discussed above: concentration ratios for analyzed plagioclase/pyroxene pairs in 64435,270 indicate that the plagioclase is poorer, or the pyroxene is richer, in REEs than would be expected for minerals crystallized from the same magma.

One possible explanation for the discrepancies may be that the phases were indeed in equilibrium with the same liquid but some of the solid–liquid Ds used for the calculation of liquid composition are not appropriate for the conditions or the composition of this system. For 64435,270, the augite Ds would have to be higher, or the plagioclase Ds would have to be lower, by a factor of three for the equilibrium liquid compositions to coincide. Relatively large variations in solid–liquid Ds caused by variations in compositions of parent liquids have been observed: for example, McKay et al. (1994) found that Ds for REEs in plagioclase in angrite meteorites are a factor of two lower than those previously determined for lunar rocks. There is no evidence, however, suggesting that the actual Ds for the plagioclase and augite of lunar rocks might differ from the Ds used herein by the required magnitude.

A more likely explanation for the discrepancies between the calculated plagioclase and pyroxene equilibrium liquids is that the plagioclase crystallized earlier than the pyroxenes so that its composition reflects equilibrium with an earlier, less REE rich, liquid. This type of difference in apparent equilibrium liquid

could have arisen in part, and perhaps even entirely, by internal diffusive homogenization of the pyroxene after crystallization (Hsu and Crozaz, 1996, 1997). In plagioclase, solid–liquid Ds for REEs do not change very much with variations in mineral composition; in pyroxenes, however, Ds show large variations that are positively correlated with variations in Ca content. Thus, zoned plagioclases would show variations related only to changes in composition of the evolving equilibrium liquid, whereas zoned pigeonites would show these variations plus variations related to increasing Ca contents. As a result, zoned pigeonite would show a much greater enrichment in REEs than co-crystallizing zoned plagioclase. Under this hypothesis, the plagioclases we selected for analysis, in the centers of grains, would preserve compositions from early in the crystallization sequence, but the pyroxenes, which would have been largely though not completely homogenized by subsolidus equilibration, would have compositions representing an average of compositions during the course of crystallization.

The hypothesis outlined above would require that the pyroxenes homogenize more readily in the subsolidus than plagioclases. Because pigeonite inversion requires a complete rearrangement of structure and composition after crystallization and plagioclases do not experience a similar process, we would expect more extensive reequilibration in pyroxenes. Unfortunately, there are little relevant data on diffusion coefficients that would permit us to evaluate this question and quantify differences. Because the trivalent REEs enter both plagioclase and pyroxene by means of coupled substitutions, the diffusion coefficients that would be most relevant would be interdiffusion coefficients for Al + REE exchanging for Ca + Si, and there are no data for these couples of elements. Available data suggest that pyroxene homogenizes more easily in major-element compositions than plagioclase: at 1200°C, the interdiffusion coefficient for CaAl-NaSi in An_{80} plagioclase (Grove et al., 1984) is an order of magnitude lower than the interdiffusion coefficient for Ca-Mg in clinopyroxene (Brady and McCallister, 1983), which is in turn two orders of magnitude lower than extrapolated interdiffusion coefficients for Mg-Fe in pyroxenes (Wilson, 1982; Rietmeijer, 1983). The only data for diffusion of REEs in pyroxenes are tracer diffusion coefficients in diopside (Sm, Sneeringer et al., 1984; Ce and Yb, Van Orman et al., 1997, 1998), and these differ by three orders of magnitude; the diffusion coefficient for Sm is similar to that for Ca-Mg in clinopyroxene cited above, the diffusion coefficient for Yb is about two orders of magnitude lower, and the diffusion coefficient for Ce is an order of magnitude lower than that for Yb. Because these are tracer diffusion coefficients rather than interdiffusion coefficients, it is not clear that they are relevant.

5.3.3. Pigeonite Distribution Coefficients

If we assume that the solid–liquid Ds for Wo_{30} augite determined by McKay et al. (1986) are correct, we can use these Ds, the analyzed composition of the primary augite, and the reconstructed composition of the primary pigeonite to calculate the solid–liquid Ds of the pigeonite (Wo_{12}) in equilibrium with the primary augite. Under this assumption, the equilibrium liquid composition calculated from the composition of the primary augite is the true equilibrium liquid composition. The pigeonite Ds determined in this manner are listed in Table 3 and plotted on Figure 8a. As discussed above, because of uncertainties as to whether or not the pigeonite and augite were in equilibrium with the same liquid or the augite was later, the pigeonite Ds determined herein are lower limits to the true Ds. The Ds determined herein are higher than those determined experimentally by McKay et al. (1986), especially for La and Ce, and the slope of the pattern is not as steep. Solid–liquid Ds for Wo_{13}, determined by the same sort of calculation using data for lunar sample 14161,7373 (Jolliff et al., 1999), agree well with the solid–liquid Ds calculated from our data (Fig. 8a), reinforcing our interpretation that the experimental Ds are too low.

In Figure 8b, we have used the pigeonite Ds derived above to recalculate the plagioclase/pigeonite concentration ratios shown in Figure 5b. In this revised plot, the shape of the pattern of predicted concentration ratios is even closer to parallel with

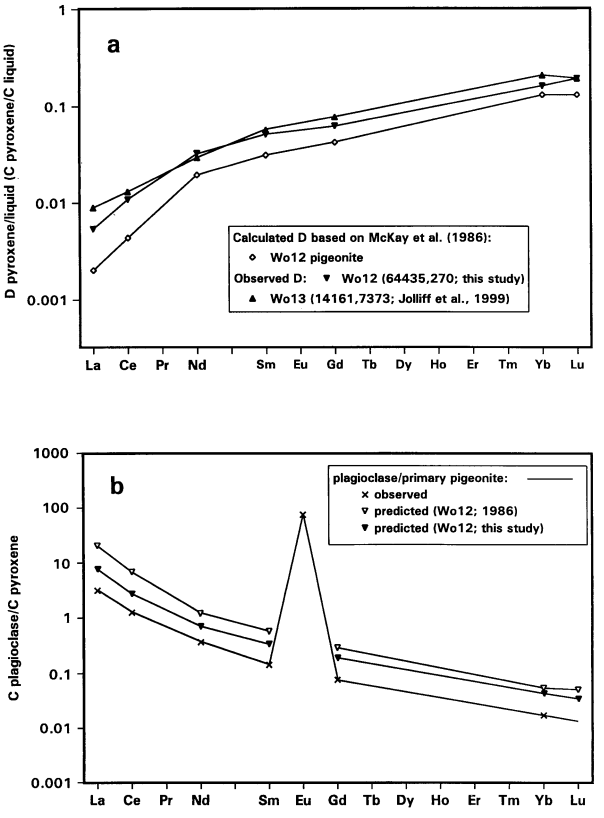

Fig. 8. Solid–liquid Ds for pigeonite and concentration ratios for plagioclase–pyroxene pairs in 64435,270. (a) Solid–liquid Ds for pigeonite. Solid–liquid Ds for pigeonite Wo_{12} were calculated from the results of this study, using solid–liquid Ds for Wo_{30} (McKay et al., 1986) and the compositions of the primary augite and reconstructed primary pigeonite in 64435,270. Solid–liquid Ds for pigeonite Wo_{13} were calculated in a similar manner from data for 14161,7373 (Jolliff et al., 1999). The results agree well and are systematically higher than solid–liquid Ds for Wo_{12} pigeonite determined experimentally by McKay et al. (1986), especially for La and Ce. (b) Measured REE concentration ratios for plagioclase/pyroxene pairs in 64435,270, compared with predicted magmatic concentration ratios for plagioclase–pyroxene pairs in equilibrium with the same liquid. The predicted magmatic patterns are derived from solid–liquid Ds listed in Table 3; Ds used for primary pigeonite are those for Wo_{12} from McKay et al. (1986) and those derived in this study.

the observed pattern of the concentration ratios. This observation reinforces the interpretation that there has been little or no subsolidus exchange of REEs between the plagioclase and the bulk inverted pigeonite.

5.4. Implications for Sm-Nd Age Systematics

The results of this study have implications for Sm-Nd age systematics. Use of a Sm-Nd isochron plot to determine crystallization age is valid only if the phases analyzed have preserved their primary REE patterns. As subsolidus reequilibration proceeds, orthopyroxene loses Nd relative to Sm as a result of diffusive exchange with nearby augite, and the Sm-Nd ratio of the mineral progressively increases. In a sample that has experienced pigeonite inversion and/or subsolidus reequilibration at a time significantly later than crystallization, a Sm-Nd isochron that is based on separates of plagioclase and orthopyroxene will indicate a lower age than the true crystallization age. Moreover, the $^{143}Nd/^{144}Nd$ intercept of the isochron at $T = 0$ will be higher than the true intercept; thus, ε_{Nd} (deviation of initial $^{143}Nd/^{144}Nd$ from chondritic) will be higher than the true ε_{Nd} at the time of crystallization. If there has been no subsolidus exchange between the plagioclase and pyroxene and the pyroxene separate has the composition of the primary pigeonite, however, the isochron age and ε_{Nd} should represent those at the time of crystallization.

Studies of Sm-Nd systematics in lunar plutonic rocks have yielded some results that have been difficult to reconcile with the results of other studies. The Sm-Nd isochron ages of lunar plutonic rocks are commonly somewhat younger than ages determined by other methods for the same rocks, and ε_{Nd} values for most lunar plutonic rocks are positive, suggesting a source depleted in LREEs relative to chondrites (Borg et al., 1998, 1999). These observations might be explained if the bulk low-Ca pyroxene analyzed in these rocks did not have the composition of the primary low-Ca pyroxene but was inversion-derived orthopyroxene, or a mixture of inversion-derived orthopyroxene and augite in which the former was present in excess. We have examined published Sm-Nd data for two ferroan anorthosites, 60025 and 62236 (Carlson and Lugmair, 1988; Borg et al., 1998, 1999), and this explanation does not appear to explain the relatively young Sm-Nd ages and positive ε_{Nd} values for these rocks because the inversion of the pigeonites in these samples was on too fine a scale to permit easy mechanical separation of the products for analysis. However, in rocks in which separation of the products of pigeonite inversion is on a coarser scale, or in rocks for which augite and orthopyroxene have been mechanically separated for analysis, it is possible that reequilibration could have significant effects on Sm-Nd results.

6. CONCLUSIONS

The results presented and discussed above lead to the following conclusions:

(1) REE patterns of pyroxenes depend upon the mode of formation of the mineral. Compared with orthopyroxene that would have crystallized from the parent liquid, orthopyroxene formed by inversion of pigeonite or by reaction of olivine with melt is significantly LREE depleted. Compared with primary augite, augite formed by inversion of pigeonite is slightly LREE depleted.

(2) As inversion of pigeonite and subsolidus reequilibration proceed, solid–solid distribution coefficients for orthopyroxene/augite progressively decrease for all REEs as the REEs move from the orthopyroxene to the augite, and the decrease is greatest for the LREEs. Thus, the REE pattern of solid–solid Ds drops and steepens as reequilibration proceeds.

(3) Solid–solid Ds depend upon temperature of reequilibration, depend upon structure of the primary mineral and may depend upon other compositional parameters as yet undetermined. There is no single set of solid–solid Ds that typifies "reequilibrated" pyroxene pairs.

(4) Compositions of equilibrium liquids calculated for pyroxenes derived by reaction of olivine or pigeonite inversion, using solid–liquid distribution coefficients, are LREE depleted relative to the true equilibrium liquids. These discrepancies arise because the phases did not crystallize directly from liquid and the use of solid–liquid Ds to calculate liquid composition is not valid. The LREE depletion is a relic of derivation of these phases from primary phases that were LREE depleted relative to their parent liquids. Thus, before calculating the composition of an equilibrium liquid from the composition of an augite or orthopyroxene, it is necessary to determine that the pyroxene is primary.

(5) If the calculated equilibrium liquid for pyroxene in a rock shows a REE pattern with a steeper positive slope than the calculated equilibrium liquid for plagioclase in the same rock, this situation is commonly interpreted as indicating that the two minerals have exchanged REEs in the subsolidus. Our results indicate that the same relationship between REE patterns of calculated equilibrium liquids can be produced simply by inversion of primary pigeonite without subsolidus exchange of REEs between plagioclase and pyroxene.

(6) Solid–liquid Ds we have determined for Wo_{12} pigeonite from our data and solid–liquid Ds we have determined for Wo_{13} pigeonite from the data of Jolliff et al. (1999) agree well and are systematically higher than those determined experimentally for shergottite pigeonites of similar Wo content by McKay et al. (1986).

(7) Solid–solid Ds calculated from literature data for terrestrial orthopyroxene/high-Ca pyroxene pairs are consistent with these pyroxene pairs having equilibrated with liquid and subsequently having reequilibrated, to varying temperatures, with each other in the subsolidus.

(8) In the ferroan anorthosites studied, the plagioclase is poorer, or the pyroxenes are richer in REEs than would be predicted from solid–liquid Ds if these mineral pairs were in equilibrium with the same magma. This discrepancy probably indicates that: 1) the plagioclase crystallized before the pyroxene; or 2) subsolidus homogenization of pyroxene has produced grains having compositions that are averages of the entire crystallization sequence, whereas lack of subsolidus homogenization of plagioclase has preserved early crystallized plagioclase at the centers of grains.

(9) The results of this study have implications for Sm-Nd studies. If the pyroxene in an analyzed sample formed by pigeonite inversion and the analyzed pyroxene separate does not have the bulk composition of the primary pigeonite but is enriched in inversion-derived orthopyroxene, the Sm-Nd age

will be younger than the true age and the ε_{Nd} will be higher than the true ε_{Nd}.

Acknowledgments—We thank Herbert Palme, Paul Warren, and an anonymous reviewer for helpful comments. This work was supported by NASA grant NAG5-9801 (C.F.) and NASA contract W-18990 (O.B.J., J.J.M.).

Associate editor: H. Palme

REFERENCES

Anders E. and Grevesse N. (1989) Abundances of the elements: Meteoritic and solar. *Geochim. Cosmochim. Acta* **53,** 197–214.

Borg L. E., Norman M., Nyquist L. E., Bogard D., Snyder G., and Taylor L. (1998) Evidence for a light-rare-earth-element–depleted source for some ferroan anorthosites. In *Origin of the Earth and Moon*, p. 2. Contribution 957. Lunar and Planetary Institute.

Borg L. E., Norman M., Nyquist L. E., Bogard D., Snyder G., Taylor L., and Lindstrom M. (1999) Isotopic studies of ferroan anorthosite 62236: A young lunar crustal rock from a light-rare-earth-element–depleted source. *Geochim. Cosmochim. Acta* **63,** 2679–2691.

Brady J. B. and McCallister R. H. (1983) Diffusion data for clinopyroxenes from homogenization and self-diffusion experiments. *Am. Mineral.* **68,** 95–105.

Cameron M. and Papike J. J. (1981) Structural and chemical variations in pyroxenes. *Am. Mineral.* **66,** 1–50.

Carlson R. W. and Lugmair G. W. (1988) The age of ferroan anorthosite 60025: Oldest crust on a young Moon? *Earth Planet. Sci. Lett.* **90,** 119–130.

Colson R. O., McKay G. A., and Taylor L. A. (1988) Temperature and composition dependencies of trace element partitioning: Olivine/melt and low-Ca pyroxene/melt. *Geochim. Cosmochim. Acta* **52,** 539–553.

Drake M. J. and Weill D. F. (1972) New rare earth element standards for electron microprobe analysis. *Chem. Geol.* **10,** 179–181.

Floss C. (1991) REE distributions in aubrites and FANs. Ph.D. thesis. Washington University, St. Louis.

Floss C. and Jolliff B. (1997) Rare earth element sensitivity factors in calcic plagioclase (anorthite). In *Secondary Ion Mass Spectrometry*, SIMS XI (G. Gillen, R. Lareau, J. Bennett and F. Stevie, Eds.), John Wiley and Sons, pp. 785–788.

Floss C., Strait M. M., and Crozaz G. (1990) Rare earth elements and the petrogenesis of aubrites. *Geochim. Cosmochim. Acta* **54,** 3553–3558.

Floss C., James O. B., McGee J. J., and Crozaz G. (1991) Lunar ferroan anorthosites: Rare earth element measurements of individual plagioclase and pyroxene grains. *Lunar Planet. Sci.* **XXII,** 391–392.

Floss C., James O. B., McGee J. J., and Crozaz G. (1998) Lunar ferroan anorthosite petrogenesis: Clues from trace element distributions in FAN subgroups. *Geochim. Cosmochim. Acta* **62,** 1255–1283.

Frey F. A. (1970) Rare earth abundances in alpine ultramafic rocks. *Phys. Earth Planet. Interiors.* **3,** 323–330.

Gromet L. P., Hess P. C., and Rutherford M. J. (1981) An origin for the REE characteristics of KREEP. *Proceedings 12th Lunar and Planetary Science Conference*, Geochimica et Cosmochimica Acta Suppl 16, pp. 903–913.

Grove T. L., Baker M. B., and Kinzler R. J. (1984) Coupled CaAl-NaSi diffusion in plagioclase feldspar: Experiments and applications to cooling rate speedometry. *Geochim. Cosmochim. Acta* **48,** 2113–2121.

Hsu W. (1995) Ion microprobe studies of the petrogenesis of enstatite chondrites and eucrites. Ph.D. thesis. Washington University, St. Louis.

Hsu W. and Crozaz G. (1996) Mineral chemistry and the petrogenesis of eucrites: I. Noncumulate eucrites. *Geochim. Cosmochim. Acta* **60,** 4571–4591.

Hsu W. and Crozaz G. (1997) Mineral chemistry and the petrogenesis of eucrites: II. Cumulate eucrites. *Geochim. Cosmochim. Acta* **61,** 1293–1302.

James O. B., Lindstrom M. M., and Flohr M. K. (1989) Ferroan anorthosite from lunar breccia 64435: Implications for the origin and history of lunar ferroan anorthosites. *Proceedings 19th Lunar Planetary Science Conference*, Cambridge University Press, Lunar & Planetary Institute, pp. 219–243.

James O. B., Lindstrom M. M., and McGee J. J. (1991) Lunar ferroan anorthosite 60025: Petrology and chemistry of mafic lithologies. *Proceedings Lunar Planetary Science*, Volume 21, Lunar and Planetary Institute, 63–87.

Jolliff B. L., Floss C., McCallum I. S., and Schwartz J. M. (1999) Geochemistry, petrology, and cooling history of 14161,7373, a plutonic lunar sample with textural evidence of granitic-fraction separation by silicate–liquid immiscibility. *Am. Mineral.* **84,** 821–837.

McKay G. A. (1989) Partitioning of rare earth elements between major silicate minerals and basaltic melts. In *Geochemistry and Mineralogy of Rare Earth Elements* (eds. B. R. Lipin and G. A. McKay), pp. 45–77. Reviews in Mineralogy 21, Mineralogical Society of America.

McKay G. A., Wagstaff J., and Yang S.-R. (1986) Clinopyroxene REE distribution coefficients for shergottites: The REE content of the Shergotty melt. *Geochim. Cosmochim. Acta* **50,** 927–937.

McKay G. A., Le L., and Wagstaff J. (1991) Constraints on the origin of the mare basalt europium anomaly: REE partition coefficients for pigeonite. *Lunar Planet. Sci.* **XXII,** 883–884.

McKay G. A., Le L., Wagstaff J., and Crozaz G. (1994) Experimental partitioning of rare earth elements and strontium: Constraints on petrogenesis and redox conditions during crystallization of Antarctic angrite Lewis Cliff 86010. *Geochim. Cosmochim. Acta* **58,** 2911–2919.

Papike J. J., Shearer C. K., Simon S. B., and Shimizu N. (1988) Lunar pyroxenes: Crystal chemical rationalization of REE zoning, pattern shapes, and abundances. *Lunar Planet. Sci.* **XIX,** 901–902.

Papike J. J., Spilde M. N., Fowler G. W., and McCallum I. S. (1995) SIMS studies of planetary cumulates: Orthopyroxene from the Stillwater Complex, Montana. *Am. Mineral.* **80,** 1208–1221.

Philpotts J. A., Schnetzler C. C., and Thomas H. H. (1972) Petrogenetic implications of some new geochemical data on eclogitic and ultrabasic inclusions. *Geochim. Cosmochim. Acta* **36,** 1131–1166.

Phinney W. C. and Morrison D. A. (1990) Partition coefficients for calcic plagioclase: Implications for Archean anorthosites. *Geochim. Cosmochim. Acta* **54,** 1639–1654.

Pun A. and Papike J. J. (1995) Ion microprobe investigation of exsolved pyroxenes in cumulate eucrites: Determination of selected trace-element partition coefficients. *Geochim. Cosmochim. Acta* **59,** 2279–2289.

Rietmeijer F. J. M. (1983) Interdiffusion coefficients parallel to c-axis in iron-rich clinopyroxenes calculated from microstructures. *Contrib. Mineral. Petrol.* **83,** 169–176.

Sack R. O. and Ghiorso M. S. (1994) Thermodynamics of multicomponent pyroxenes: II. Phase relations in the quadrilateral. *Contrib. Mineral. Petrol.* **116,** 287–300.

Schnetzler C. C. and Philpotts J. A. (1970) Partition coefficients of rare-earth elements between igneous matrix material and rock-forming mineral phenocrysts –II. *Geochim. Cosmochim. Acta* **34,** 331–340.

Shearer C. K., Papike J. J., Simon S. B., and Shimizu N. (1989) An ion microprobe study of the intra-crystalline behavior of REE and selected trace elements in pyroxene from mare basalts with different cooling and crystallization histories. *Geochim. Cosmochim. Acta* **53,** 1041–1054.

Sneeringer M., Hart S. R., and Shimizu, N. (1984) Strontium and Samarium diffusion in diopside. *Geochim. Cosmochim. Acta* **48,** 1589–1608.

Stosch H.-G. (1982) Rare earth element partitioning between minerals from anhydrous spinel peridotite xenoliths. *Geochim. Cosmochim. Acta* **46,** 793–811.

Sun M. and Kerrich R. (1995) Rare earth element and high field strength element characteristics of whole rocks and mineral separates of ultramafic nodules in Cenozoic volcanic vents of southeastern British Columbia, Canada. *Geochim. Cosmochim. Acta* **59,** 4863–4879.

Tanaka T. and Aoki K.-I. (1981) Petrogenetic implications of REE and Ba data on mafic and ultramafic inclusions from Itinome-gata, Japan. *J. Geol.* **89,** 369–390.

Van Orman J. A., Shimizu N., and Grove T. L. (1997) Diffusion of Ce and Yb in diopside: Disequilibrium effects on rare earth element

patterns in high-Ca pyroxenes in abyssal peridotites (abstract). *Trans. Am. Geophys. Union* **78,** F836.

Van Orman J. A., Grove T. L., and Shimizu N. (1998) Uranium and thorium diffusion in diopside. *Earth Planet. Sci. Lett.* **160,** 505–519.

Weill D. F. and McKay G. A. (1975) The partitioning of magnesium, iron, strontium, cerium, samarium, europium, and ytterbium in lunar igneous systems and a possible origin of KREEP by equilibrium partial melting. *Proceedings 6th Lunar Science Conference*, Geochimica et Cosmochimica Acta Suppl. 6, Pergamon Press, pp. 1143–1158.

Wilson A. H. (1982) The geology of the Great "Dyke," Zimbabwe: The ultramafic rocks. *J. Petrol.* **23,** 240–293.

Zinner E. and Crozaz G. (1986) A method for the quantitative measurement of rare earth elements in the ion microprobe. *Intl. J. Mass Spec. Ion. Proc.* **69,** 17–38.